Strontium and sulphur isotopic constraints on the formation of the Mangampeta barite deposit, Cuddapah basin

Bivin Geo George[1], N. Shalini[1], M. S. Pandian[1], Vinai K. Rai[2], Rajneesh Bhutani[1,*] and S. Balakrishnan[1]

[1]Department of Earth Sciences, Pondicherry University, Puducherry 605 014, India
[2]Planetary Science Division, Physical Research Laboratory, Ahmedabad 380 009, India

Strontium (Sr) isotope analyses of barite and associated pyrite-bearing carbonaceous tuff are carried out to understand the nature of mineralizing fluids for Mangampeta barite deposit, which is one of the largest barite deposits in the world. $^{87}Sr/^{86}Sr$ ratios of barite and pyrite-bearing carbonaceous tuff range from 0.70754 to 0.728951 and 0.72969 to 0.819633 respectively. These ratios, high compared to the Proterozoic sea water, preclude the well-mixed sea water or mantle to be the immediate source of Sr, and by association of barium (Ba). We infer that Sr and Ba were derived from the Cuddapah sediments by a sedimentary exhalative process. This is further substantiated by the fluid inclusions in the barites which yield a limited range of salinity, but a wide range of homogenization temperatures (from 300°C to 120°C), indicating that ore deposition took place due to cooling of hydrothermal fluid with limited mixing of ambient sea water, thereby preserving the salinity as well as Sr isotope ratios of the ore fluid.

The relative sulphur isotope ratios ($\delta^{34}S$) reported from the barites of Mangampeta fall in a narrow range 41.3–45.5‰, whereas the $\delta^{34}S$ of pyrites falls in two distinct categories. Pyrites with $\delta^{34}S$ close to 0‰ are interpreted to have formed by magmatic S acquired by the hydrothermal fluid, whereas pyrites with $\delta^{34}S$ values ranging from 8.1‰ to 38.8‰ are the result of biogenic reduction of sea-water sulphate.

Keywords: Barite, Cuddapah basin, sedex deposits, strontium and sulphur isotopes ratios.

BARITE deposits are classified based on the source of barium (Ba): (i) marine or pelagic barite in which Ba is released from degradation of organic matter; (ii) hydrothermal barite where Ba enters the hydrothermal fluid formed as a result of hydrothermal activity; (iii) cold seeps barite where Ba is supplied from the sediments by tectonic or hydrologic process and (iv) diagenetic barite where Ba is added to pore fluid during diagenetic process[1,2]. Sea water supplies SO_4^{2-} in the first three modes of precipitation, whereas a decrease in solubility controlled by pressure and temperature of the fluid results in the precipitation of diagenetic barite.

The bedded barite deposit at Mangampeta is one of the largest barite deposits in the world. This deposit consists of granular and lapilli forms of barite intercalated with carbonaceous shale and tuff, of which, granular barite formed by precipitation of hydrothermal exhalative under submarine conditions and the radial platy lapilli type is attributed to the pyroclastic phase of volcanism[3,4]. Minor amount of barite occurs in fracture-filling veins in the underlying dolostone[3,4].

During the precipitation of barite from aqueous fluid, strontium (Sr) in trace quantities substitutes for barium in the crystal structure of barite due to similarity in ionic radius and electronegativity. Some amount of carbonate is also precipitated along with the barite, both having the same Sr isotope ratios. The $^{87}Sr/^{86}Sr$ ratio carries clues regarding the source of barium[1,2,5,6]. Since rubidium is incompatible in barite and carbonate crystal structures, the ^{87}Sr present in barite and co-precipitated carbonates does not change with time and thus gives information about source of the fluid[1,2]. A previous study on the bedded barite deposit of Mangampeta has shown $^{87}Sr/^{86}Sr$ ratios ranging from 0.70708 to 0.71626, indicative of derivation of Sr from the older continental crust[7].

Sulphur (S) isotope studies of the Mangampeta barite and associated pyrite suggested that the sulphur was derived from sea-water sulphate with initial $\delta^{34}S$ at 25–30‰, same as Proterozoic sea water, later enriched in $\delta^{34}S$ by bacterial reduction in the ocean basin[4,8–10]. Highly enriched $\delta^{34}S$ value (41.3–45.5‰) of the Mangampeta barite resulted due to progressive reduction of sulphate to pyrite in a closed system that enriched the $\delta^{34}S$ of the remaining dissolved sulphate[4,8–10]. High $\delta^{34}S$ values of Mangampeta pyrites (8.1–38.8‰) and the associated large spread, indicate progressive bacterial reduction. Sarkar *et al.*[9] carried out sulphur isotope analyses of barite and associated pyrites of Mangampeta deposits along with similar deposits from other Proterozoic basins of India. They have proposed, based on high sulphur isotope ratios of pyrites, that there has been a global anoxic condition during the deposition of these pyrites. However, $\delta^{34}S$ values of pyrites as low as 0 ± 2‰ are also reported from Mangampeta and other basins[7,8]. We report here results on Sr isotope composition of barite, pyrite and dolostone of Mangampeta and interpret these along with previously reported S isotope ratios to provide additional constraints on the nature of formation fluids of the barite deposit.

Mangampeta barite deposit is situated in the southern part of the Mesoproterozoic Cuddapah basin (Figure 1). The barite deposit is confined to the Pullampet Formation of Cheyair Group of Cuddapah Supergroup. The Pullampet Formation consists of shale intercalated with dolostone and quartzite[3].

*For correspondence. (e-mail: rbhutani@gmail.com)

The bedded barite deposit occurs in Pullampet shale as two lenticular bodies occupying troughs of two synclines which are separated about 700 m by an anticline. The two lenses, named as northern lens and southern lens, are respectively 750 and 200 m long[3]. The northern lens has a maximum thickness of 44 m and the southern lens is 12 m at the centre and tapers towards the edges. The beds have a general NNW–SSE strike and dip moderately towards ENE[3,8]. The general order of superposition of strata is given in Figure 2. Granular barite forms the lowermost horizon of the barite deposit underlain by carbonaceous tuff and dolomite. Lapilli barite overlies the granular one.

About 50 mg aliquots of powdered barite samples, collected from the northern lens of the Mangampeta deposit, were taken in vials and leached using 1 M acetic acid (Sea Star™) at 70°C for 3 h. Acetic acid mainly attacks carbonates co-precipitated with barite. Intermittently solutions were ultrasonicated for 1 h. The sample was centrifuged and the solution was decanted. The solution was then transferred to PTFE vial and evaporated. It was further treated with 2 ml of 6 N HNO_3 and dried. Finally samples were redissolved in 2 ml of 3 N HNO_3. The solution was then loaded in 200 µl of preconditioned Sr-specific resin (52–100 µm) from Eichrom™ filled in 2 ml polypropylene (PP) columns. Matrix elements were eluted by washing with 5 ml of 3 N HNO_3 followed by elution of Sr with 5 ml of MilliQ™ water. Appropriate amount of 1.5 N HNO_3 was added to make the solution to 0.3 N HNO_3 for MC–ICPMS analysis. Sr isotope analyses for barite samples were performed on Thermo Neptune MC–ICPMS at the Physical Research Laboratory, Ahmedabad. Each sample was measured for 60 cycles with 8 sec integration time. ^{83}Kr, ^{84}Sr, ^{85}Rb, ^{86}Sr, ^{87}Sr and ^{88}Sr peaks were monitored on cups L3, L2, L1, C, H1 and H2 respectively. All the data were corrected for mass bias with $^{88}Sr/^{86}Sr$ value of 8.3752 using the exponential law ^{85}Rb never exceeded 10^{-2} V. After every four or five samples, NIST NBS 987 Sr was analysed in different concentrations (from 40 to 200 ppb) to check the accuracy and precision of measurements. The average value of $^{87}Sr/^{86}Sr$ obtained in three repeat measurements is 0.710296, with standard error of 0.000008.

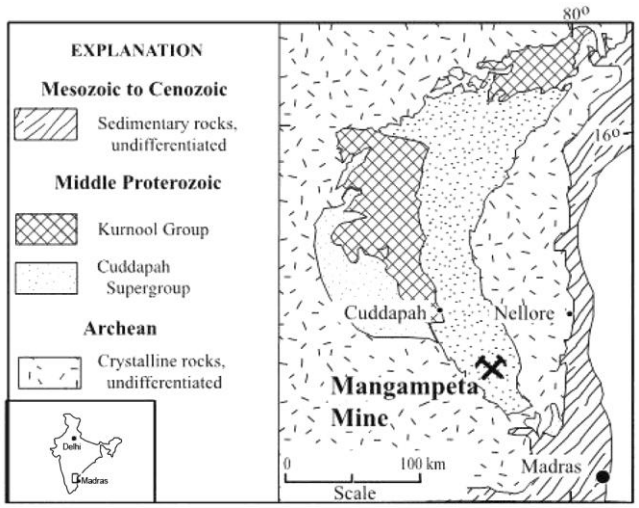

Figure 1. Regional map of Cuddapah basin showing Mangampeta barite deposit (from Clark *et al.*[4]).

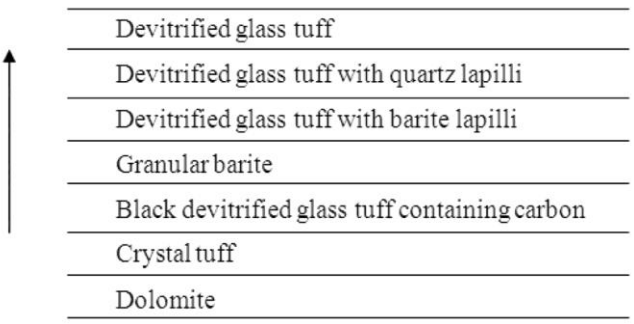

Figure 2. Geological succession of the Mangampeta barite deposit (after Kurien *et al.*[3]).

Fluid inclusion studies were carried out at Pondicherry University on the doubly polished wafer sections of about 500–200 µm thickness. Linkam THMS 600 heating–freezing stage, which is attached to a polarizing microscope, was used for the microthermometry in the temperature range –196°C to +600°C. Inclusions were frozen using pre-chilled N_2 gas and pre-heated compressed air was used for heating. The unit was calibrated using synthetic H_2O–CO_2 inclusions and pure CO_2 inclusions (triple point –56.6°C). The accuracy of the system is ~0.1°C during freezing and ~1°C during heating. Homogenization temperature of inclusions was determined during heating. By gradual heating of inclusions, vapour bubble size reduces and disappears. The temperature at which the vapour bubble disappears corresponds to homogenization temperature of the inclusion.

The $^{87}Sr/^{86}Sr$ ratios of barite and associated pyrite-bearing carbonaceous tuff (Table 1) show a wide range of values ranging from 0.707540 (for a sample of granular barite) to 0.819633 (for a sample of pyrite-bearing tuff). All three types of barites – granular, lapilli and vein show higher ratios than the $^{87}Sr/^{86}Sr$ ratio of the Proterozoic sea water, which points to a continental source. Crawford and Compston[11] report $^{87}Sr/^{86}Sr$ initial ratio in the range 0.707–1.104 from the igneous intrusions into the Nallamalai sediments. These intrusions are younger than the barite deposit and therefore could not have contributed Sr to the barite deposit. It is most likely that a continental basement or basement-derived sediments with high $^{87}Sr/^{86}Sr$ ratio might have acted as a source to the anomalous values observed in the Mangampeta barite. Preliminary results from our ongoing measurements of Sr isotope ratios of the dolostone which underlies the barite beds point towards higher $^{87}Sr/^{86}Sr$ ratios, similar to that of barite, indicating that sediments associated with barite

Table 1. Strontiun isotope ratio of the Mangampeta barite and associated pyrite-bearing carbonaceous tuff. Errors (2σ) in the $^{87}Sr/^{86}Sr$ ratio are errors in the last decimal place

Sample	Remarks	$^{87}Sr/^{86}Sr$
MGP 10	Granular barite	0.711676 ± 8
MN 11A 19	Barite lapilli in barite lode	0.719798 ± 4
MN 11A 16	Barite vein in dolostone	0.717003 ± 8
MN 11A 18	Barite lapilli in carbonaceous tuff	0.72895 ± 14
MN 10A 06	Granular barite	0.707540 ± 8
MN 11A 20	Barite lode with pyrite grains	0.719409 ± 8
MN 11A 18A	Barite lapilli with pyrite grains in carbonaceous tuff	0.729969 ± 8
MS 11 01B	Pyrite lens in carbonaceous tuff	0.75589 ± 6
MN 11A 17A	Pyrite lens in carbonaceous tuff	0.81963 ± 1
MN 11A 17B	Pyrite nodules in carbonaceous tuff	0.79204 ± 2
Cody shale		0.709448 ± 6

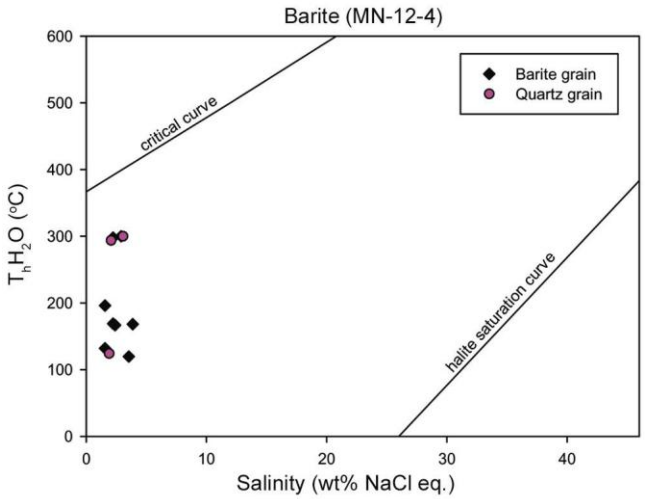

Figure 3. Homogenization temperature versus salinity plot of aqueous bi-phase inclusions in barite and quartz from bedded barite deposit. The trend indicates simple cooling of the ore fluid with minimal mixing with the ambient sea water[12].

can be a source of the radiogenic Sr. Barite beds at Mangampeta are intercalated with carbonaceous shale and tuff which would also have radiogenic Sr. However, detrital input could not have had much effect on the sea water $^{87}Sr/^{86}Sr$ ratio in case Sr was completely mixed. Therefore, there are two possible scenarios of depositional environment of barite that could be consistent with the observed Sr isotopic ratios. The first is that the basin was isolated and remained closed, as also suggested previously[8], in such a way that the $^{87}Sr/^{86}Sr$ isotope ratio of water could be changed towards continental values. This is possible if the deposition of barite took place during active rifting and opening of the basin. The second possibility is that Ba derived from continental sediments, through hydrothermal fluid, precipitated as barite without significant mixing with sea water. This indicates that influx of Ba-rich fluid was contemporaneous with the influx of radiogenic continental Sr, or both the elements were derived from the same source rocks. This is the sedimentary exhalative process in which the hydrothermal fluid, while traversing through the sediments, leaches Ba and Sr and barite deposition takes place on its discharge into the sea.

Considering the above two scenarios, sedimentary exhalative process seems to be the more likely scenerio, which has also been suggested as the mode of origin for similar bedded barite deposits from the other geographical locations of the world[4,6].

Further, the results from our ongoing fluid inclusion studies also indicate that the deposition of bedded barite took place due to cooling of hydrothermal fluid upon entry into sea with minimal mixing with the ambient sea water. Microthermometric analysis of primary aqueous bi-phase inclusions present in barite and associated quartz from the bedded barite deposit reveals a wide range of homogenization temperatures (T_h) from 120°C to 300°C, and a narrow range of salinity (1.57–3.87 wt% NaCl equivalent; Figure 3). In aqueous bi-phase ($L + V$) inclusions, T_h ($L + V - L$) is considered to be the lower limit of crystallization temperature of the growing crystal during entrapment of the fluid. A wide range of T_h and narrow range of salinity is indicative of crystallization during cooling of the hydrothermal fluid with minimal mixing of the ambient sea water[12]. This favours the scenario in which Sr is incorporated into barite without mixing with sea water, thereby preserving the signature of the source rocks through which the hydrothermal fluid circulated before exhalation on the seafloor.

Sulphur isotope composition of pyrites of Mangampeta shows two distinct $\delta^{34}S$ values (Table 2 and Figure 4). One set of values belongs to the range +8.1‰ to +38.8‰ (ref. 9), where pyrite formation is by bacterial sulphate reduction and the other is in the range –1.1‰ to 0.0‰ (ref. 8). The $\delta^{34}S$ value of barite shows a consistent narrow range +41.8 to +45.5‰, which is the result of bacterial sulphate reduction (Figure 6). In general, biogenic pyrites have framboidal texture, while magmatic pyrites occur as discrete euhedral grains. However, under certain circumstances framboidal pyrites can be completely converted into homogenous euhedral pyrite[13]. Petrographic

Table 2. Published δ^{34}S data of Mangampeta barite and pyrites given relative to Canyon Diablo Troilite

δ^{34}S pyrite (‰)	δ^{34}S barite (‰)	Location	Reference
	41.8–45.5 (seven samples)	Laminated black shale – barite	4, 10
	42.3	Laminated black shale – barite	9
8.1		Laminated black shale – pyrite	9
38.3		Laminated black shale – pyrite	9
38.8		Laminated black shale – pyrite	9
25.3		Laminated black shale – pyrite	9
	43.5	Barite lapilli – rosette type	8
0		Carbonaceous layer at the base of barite	8
–1.1		Carbonaceous layer at the base of barite	8
2.5	45.5	Alternate layers of barite lapilli-tuff and tuff	8
	42.3	Bedded barite	8

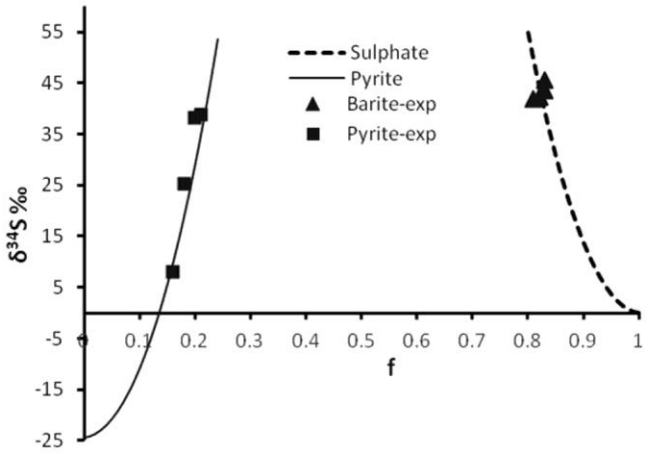

Figure 4. Rayleigh's distillation curves calculated for bacterial fractionation between sulphate and pyrite of Mangampeta. *f* is the fraction of sulphate remaining in the basin (for barite curve) and the complementary fraction of sulphide generated (for pyrite curve). Fractionation factor (sulphate to sulphide) is taken as $\alpha = 1.025$ for closed system. The triangular and square dots represent the experimental values reported for barites and pyrites.

study of the Mangampeta succession shows the presence of euhedral pyrite in carbonaceous tuff and barite veins that form the basal part of bedded barite (Figure 5). In addition, replacement type of barite was also reported[3], where barite grains replace pyrite and quartz along grain margins in the basal dolomite and tuff of the Mangampeta succession (Figure 5). This clearly indicates the existence of genetically different sets of pyrite in the basin. Current understanding of the Mangampeta barite deposition does not explain two generations of pyrites and therefore requires a fresh look into the system.

Cuddapah, an intracratonic rift basin, had periodic subsidence[14] as implied by the repeated occurrence of alternate quartzite, shale and limestone beds. The rift-related faults are likely to control the circulation of the hydrothermal fluids which dissolve Sr from sediments as indicated by the higher $^{87}Sr/^{86}Sr$ ratios.

Geochemical modelling of the existing sulphur isotope data has been done based on the fact that only multiple episodes of redox conditions can explain the presence of two generations of pyrite. To start with, the initial sulphur was supplied to the basin through hydrothermal process related to rifting. This sulphur has δ^{34}S nearly zero[15], which under the reducing conditions in the basin formed the first-generation euhedral pyrite. The stratigraphic position of this generation of pyrite at the basal part of the barite deposit, its low δ^{34}S value and its existence with carbonaceous tuff reiterates the reducing conditions envisaged in the model.

Subsequently in an emerging oxic scenario, sulphides were oxidized to sulphates. This oxidation could be a purely inorganic and quantitative process and therefore does not fractionate the sulphur isotopes significantly[16]. Subsequent anoxic condition leading to the progressive biogenic reduction of sulphate available in sea water explains the higher δ^{34}S values observed in barite (+41.8‰ to +45.5‰) and a wide range of values observed in the second-generation biogenic pyrite (+8.1‰ to +38.8‰; Figure 4). This process has been modelled using simple Rayleigh distillation model[17], which shows a sulphate to pyrite reduction limited to 17–20% of the total (Figure 4). The δ^{34}S values of pyrite are also consistent with the extent of fractionation. The observation is also supported by the fact that a massive amount of barite is present in the basin commensurate with the residual sulphate after the biogenic reduction. The wide range of δ^{34}S values in pyrite may tempt one to suggest that both the first- and second-generation pyrites are a result of bacterial sulphate reduction; but the difference in the δ^{34}S values of the two types of pyrite and the petrographic evidence for the presence of euhedral, non-biogenic pyrites in basal dolostone marks the distinction. The bacteriogenic pyrite is generally associated with carbonaceous shale.

The strontium isotope analyses of barites and associated pyrite-bearing carbonaceous tuff of Mangampeta show high $^{87}Sr/^{86}Sr$ ratio. The anomalous values are attributed to continental sources. Terrestrial sources alone cannot contribute to such a high ratio, if the basin was well-mixed before barite deposition. Hence it is inferred

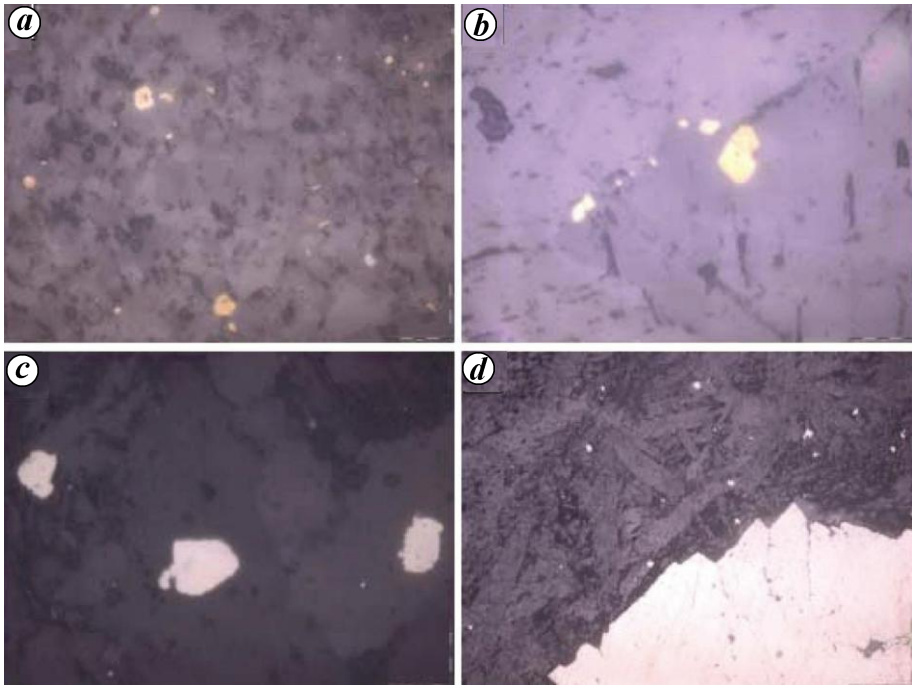

Figure 5. ***a***, Euhedral crystals of pyrite and chalcopyrite in barite vein. ***b***, Chalcopyrite in barite vein. ***c***, ***d***, Pyrite in dolostone. Width of ***a***–***c***, 3.5 mm, width of ***d***, 35 mm.

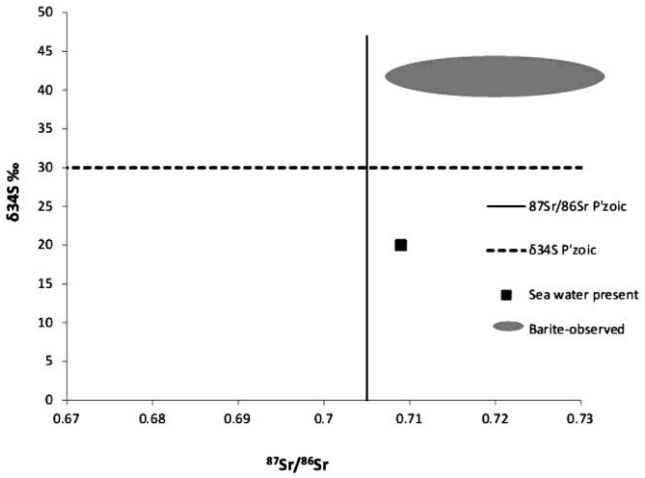

Figure 6. δ^{34}S versus Sr isotope ratio of the Mangampeta barite (^{87}Sr/^{86}Sr ratio from the present analysis and δ^{34}S of barites from refs 4, 8–10). The lines parallel to the *x* and *y* axes represent the δ^{34}S and ^{87}Sr/^{86}Sr ratio of the Proterozoic sea water respectively. The grey ellipse represents the range of values observed for barites and the square dot indicates the present-day sea-water values.

that Ba and Sr were mobilized by hydrothermal fluid from the sediments and barite deposition took place by sedimentary exhalative process.

The reported δ^{34}S values of pyrites from Mangampeta fall into two distinct categories. This might be because of multiple redox conditions prevalent during basin development. Pyrites with δ^{34}S nearly zero are formed during the initial phase of rifting from anoxic hydrothermal fluid. These are the first-generation pyrites formed under reducing conditions and are seen mostly at the base of barite deposit. Petrographic study indicates these are replaced by barite grains along margins. Bacterial reduction of sea-water sulphates under local reducing conditions produced the second-generation pyrites which typically show higher δ^{34}S values and are dispersed in the carbonaceous shale. Raleigh fractionation model indicates that 17–20% of sulphates was reduced to pyrite.

1. Griffith, E. M. and Paytan, A., Barite in the ocean – occurrence, geochemistry and palaeoceanographic applications. *Sedimentology*, 2012, **59**, 1817–1835.
2. Paytan, A., Mearon, S., Kobb, K. and Kastner, M., Origin of marine barite deposits: Sr and S isotope characterization. *Geology*, 2002, **30**, 747–750.
3. Kurien, T. K., Setti, D. N., Neelakantam, S., Suthanandam, S. and Roy, S., Baryte mineralization and its origin, Mangampeta, Cuddapah district, Andhra Pradesh. *Indian Mineral.*, 1977, **18**, 1–6.
4. Clark, H. B., Poole, F. G. and Wang, Z., Comparison of some sediment-hosted, stratiform barite deposits in China, the United States, and India. *Ore Geol. Rev.*, 2004, **24**, 85–101.
5. Faure, G., *Principles of Isotope Geology*, John Wiley, 1986, 2nd edn.
6. Jewell, P., Bedded barite in the geologic record. In *Marine Authigenesis: From Global to Microbial*, Society for Sedimentary Geology Special Publication No. 66, 2000, pp. 147–161.
7. Mukherjee, A. and Prabhakar, G., Fluid inclusion studies and sulphur and strontium isotope geochemistry of vein barites of Velugumetla, Khammam district, Andhra Pradesh. *J. Geol. Soc. India*, 2006, **68**, 201–206.
8. Karunakaran, C., Sulphur isotopic composition of barite and pyrites from Mangampeta, Cuddapah district, Andhra Pradesh. *J. Geol. Soc. India*, 1976, **17**, 181–185.
9. Sarkar, A., Chakraborty, P. P., Mishra, B., Bera, M. K., Sanyal, P. and Paul, S., Mesoproterozoic sulphidic ocean, delated oxygena-

tion and evolution of early life: sulphur isotope clues from Indian Proterozoic basins. *Geol. Mag*., 2010, **147**, 206–218.
10. Clark, S. H. B. and Basu, P. K., Geologic setting and origin of the Mangampeta barite deposit, India. In *Mineral Deposits: Processes to Processing* (eds Stanley, C. J. *et al.*), Balkema, Rotterdam, The Netherlands, 1999, pp. 1085–1088.
11. Crawford, A. R. and Compston, W., The age of the Cuddapah and Kurnool systems, southern India. *J. Geol. Soc. Aust.*, 1973, **19**, 453–464.
12. Shepherd, T. J., Rankin, A. H. and Alderton, D. H. M., *A Practical Guide to Fluid Inclusion Studies*, Blackie, New York, 1985, p. 239.
13. Ostwald, J. and England, B. M., The relationship between euhedral and framboidal pyrite in base-metal sulphide ores. *Mineral. Mag.*, 1979, **43**, 297–300.
14. Ramam, P. K. and Murty, V. N., *Geology of Andhra Pradesh*, Geological Society of India, 1997, p. 245.
15. Thode, H. G., Monster, J. and Dunford, H. B., Sulphur isotope geochemistry. *Geochim. Cosmochim. Acta*, 1961, **25**, 159–174.
16. Allegre, C. J., *Isotope Geology*, Cambridge University Press. 2008, p. 512.
17. Seal, R. R., Sulfur isotope geochemistry of sulfide minerals. *Rev. Mineral. Geochem.*, 2006, **61**, 633–677.

ACKNOWLEDGEMENTS. We thank the anonymous reviewers whose in-depth reviews have been helpful in improving the manuscript. We also thank R. Ramesh who helped us improve the language of the manuscript.

Received 12 December 2012; revised accepted 15 May 2013

Field evaluation of 3D geo-electrical resistivity imaging for environmental and engineering studies using parallel 2D profiles

A. P. Aizebeokhai[1] and V. S. Singh[2,*]

[1]Department of Physics, Covenant University, Ota, Nigeria
[2]CSIR-National Geophysical Research Institute, Hyderabad 500 007, India

Eight parallel two-dimensional (2D) geo-electrical resistivity profiles were generated in hard-rock (Pulivendla) area of Andhra Pradesh, India using a Lund imaging multi-electrode system adopting Wenner array. The aim of the survey was to experimentally evaluate the effectiveness of using parallel 2D profiles for three-dimensional (3D) geo-electrical resistivity imaging for better understanding of aquifer geometry and its characteristics. The observed 2D apparent resistivity data were independently inverted, and then collated to 3D data set. The inversion of the resulting 3D data set was carried out using a full 3D inversion code. The 3D inverse model of resistivity images obtained are presented as horizontal depth slices. The 2D images extracted from 3D inverse models showed no distortions that are observed in 2D models obtained by 2D inversion. The 3D inverse model resistivity appears to be more realistic, considering the hydrogeology of the area. The unusually high resistivity values observed in the 2D inverse models were not observed in the 3D inverse models. The very low near-surface inverse model resistivity observed is thought to be structurally influenced. The results, which are consistent with numerical evaluation, show that high resolution 3D geoelectrical resistivity imaging can be successfully conducted using parallel 2D profiles if appropriate survey parameters are carefully chosen.

Keywords: Field evaluation, 2D and 3D imaging, 3D inversion, parallel 2D profiles, resistivity survey.

GEOELECTRICAL resistivity imaging has been used to address a wide variety of hydrological, environmental and engineering problems. Subsurface geology in many hydrological, environmental and engineering sites is often subtly heterogeneous and on multi-scale, such that the variations of the subsurface properties can be very rapid and erratic. Two-dimensional (2D) geo-electrical resistivity imaging is often used to investigate areas with such complex subsurface geology[1–5]. In 2D resistivity surveys, subsurface resistivity is usually assumed to vary vertically with depth and laterally along the profile, but constant in the direction perpendicular to the profile. However, subsurface features are inherently three-dimensional (3D). Thus, the 2D assumption is commonly violated. The violation of the 2D assumption often leads to out-of-plane resistivity anomaly in the 2D inverse models and this could be misleading in the interpretation of subsurface features[6,7]. Thus, a 3D geo-electrical resistivity imaging which allows resistivity variation in all possible directions should give more accurate and reliable inverse models of the subsurface resistivity. 3D geo-electrical resistivity imaging can be used to characterize the heterogeneity of aquifer system, which allows for better understanding of groundwater flow and management. In addition, 3D geo-electrical resistivity imaging can be used to plan monitoring of groundwater flow at the sites of more focused studies, such as, nuclear installations, landfill sites and waste disposal sites which often requires 3D definition of the aquifer geometry and characterization. It has also been used in archaeological studies, treasure hunt, detection of underground leakages, etc.

The techniques for conducting 3D resistivity surveys have been presented by Loke and Barker[8]. Square and rectangular grids of electrodes with constant electrode spacing in both *x*- and *y*-directions are commonly used[8–12]. Each electrode in the grid is in turn used as the current electrode while the potential difference is measured at all other electrode positions. However these techniques,

*For correspondence. (e-mail: vssingh77@hotmail.com)